Self-Calibrated Coherent Optical Vector Analysis With High Resolution and Sensitivity

Lihan Wang, Huashan Yang, Xiangchuan Wang, Xiaohu Tang, Jingxian Wang, Qianwen Sang, Min Xue, and Shilong Pan, *Fellow, IEEE*

***Abstract*— Measurement of the frequency response of sensors and devices with high-frequency resolution and sensitivity is of great importance for high-sensitive trace gas detection, high-quality photonic circuit fabrication, etc. Optical vector analysis (OVA) based on microwave photonics (MWPs) offers outstanding frequency resolution. However, the sensitivity of the incoherent detection system is usually limited. This article proposes a self-calibrated coherent OVA system that leverages MWP technology. The laser phase noise, which is the leading challenge in coherent detection, is compensated through a self-calibration process. Employing precise microwave sweeping paired with a highly stable laser, the proposed system achieves a theoretical frequency resolution at the level of hertz. In the experiments, we demonstrate a sensitivity improvement of at least 35 dB over the incoherent system. In addition, the proposed OVA system offers superior frequency resolution and accuracy compared to commercial coherent OVA products.**

***Index Terms*— Coherent detection, frequency response measurement, optical vector analysis (OVA), self-calibration.**

I. Introduction

FREQUENCY response characterizes how a device or system reacts to various signal frequencies, directly representing the physical properties inherent in devices [1], [2], [3], [4] and substances [5], [6], [7], [8]. For example, as photonic-integrated circuits develop [9], [10], [11], [12], [13], an increasing number of devices and new materials require high-accuracy and high-resolution frequency response measurements for adequate performance characterization. In addition, in optoelectronic systems, precise spectrum manipulation has been proven to be an effective method for signal generation and processing [14], [15], [16], [17]. Measurement schemes that rely on spectral response analysis for precise metrology or characterization of specific parameters typically require exceptionally high sensitivity and resolution to ensure accurate and reliable results [18], [19].

Received 6 October 2024; revised 16 February 2025; accepted 27 February 2025. Date of publication 18 March 2025; date of current version 2 April 2025. This work was supported in part by the National Natural Science Foundation of China under Grant 62271249 and Grant 62075095, in part by the Fundamental Research Funds for the Central Universities under Grant NC2024004, and in part by the Funding for Outstanding Doctoral Dissertation in Nanjing University of Aeronautics and Astronautics (NUAA) under Grant BCXJ24-09. The Associate Editor coordinating the review process was Dr. Valentina Bello. *(Corresponding authors: Xiangchuan Wang; Shilong Pan.)*

The authors are with the National Key Laboratory of Microwave Photonics, Nanjing University of Aeronautics and Astronautics, Nanjing 210016, China (e-mail: andwwlh@nuaa.edu.cn; wangxch@nuaa.edu.cn; pans@nuaa.edu.cn).

Digital Object Identifier 10.1109/TIM.2025.3552382

Optical vector analysis (OVA) is a technology capable of performing multidimensional frequency response measurements, encompassing magnitude, phase, and group delay responses. Traditional OVA systems can be categorized into two types: based on incoherent demodulation [20], [21], [22], [23] and coherent demodulation [24], [25], [26], [27], [28], [29], [30], [31], [32], [33]. In incoherent OVA systems, the response of the device under test (DUT) is directly mapped onto changes in the amplitude envelope of the probe light. The probe light is then converted into the photocurrent, facilitating the demodulation of the DUT response [22]. Previously, the highest performance achieved by an incoherent OVA system utilizing microwave photonic (MWP) technology [23] was validated with a frequency resolution of 334 Hz, a frequency range of 1.034 THz, and a dynamic range of 90 dB. Nevertheless, the incoherent OVA is susceptible to the insertion loss of the DUT owing to its reliance on direct detection in the photoelectric conversion process, limiting its application. For example, the transmission loss on a silicon-on-insulator platform is typically around 3 dB/cm, and the coupling loss of the grating couplers on such a platform usually exceeds 4 dB [34]. The total insertion loss for a chip with complex functions can exceed 20 dB [35], [36], [37]. For trace gas detection [38], probe light must undergo repeated reflections within the gas cell to amplify the absorption peak's amplitude [39], which can lead to even higher losses. Consequently, the incoherent OVA system demonstrates limited applicability in scenarios that require high sensitivity. The avalanche photodiode (APD) [40] has been widely recognized as an effective solution to improve receiver sensitivity, due to its substantial internal gain. However, the inherent coupling of amplitude and phase [41] in APD can lead to considerable measurement errors.

Coherent OVA systems provide better sensitivity than incoherent OVA systems. The local oscillator (LO) signal plays a crucial role in these systems, compensating for power loss, and thus enhancing the system's sensitivity. Swept-frequency interferometry [24], [25], [26], [27], [28] is the most commonly employed method in the coherent systems, where the response of the DUT is mapped onto the amplitude and phase of the interference signal. However, since the LO and probe signal traverse different paths, laser phase noise can be introduced into the interference signal, potentially degrading the measurement accuracy. Furthermore, the swept-frequency interferometry method features a limited frequency resolution, generally around 200 MHz [42]. This limitation is primarily

1557-9662 © 2025 IEEE. All rights reserved, including rights for text and data mining, and training of artificial intelligence and similar technologies. Personal use is permitted, but republication/redistribution requires IEEE permission.
See https://www.ieee.org/publications/rights/index.html for more information.
Authorized licensed use limited to: NANJING UNIVERSITY OF AERONAUTICS AND ASTRONAUTICS. Downloaded on August 19,2025 at 09:01:27 UTC from IEEE Xplore. Restrictions apply.

due to the poor stability and low wavelength repeatability of the tunable laser used in the system. Researchers have proposed a range of technologies to address laser phase noise in coherent OVA systems. An approach involves establishing an auxiliary interferometer to capture the real-time phase fluctuation and frequency drift of the laser [25], [26], [27], [28]. It is crucial to shield the auxiliary interferometer from external environmental influences. Otherwise, any drift in the interferometer could adversely affect the measurement accuracy.

Some researchers have explored the combination of MWP-based methods with coherent OVA systems to obtain high sensitivity and frequency resolution simultaneously [29], [30], [31], [32], [33]. In [29], the phase response is deduced from the magnitude response using the Kramers–Krönig relation. Although this method circumvents the need for direct phase extraction, its applicability is limited to devices under test (DUTs) that conform to minimum-phase system criteria, restricting the measurement scenarios. Another approach involves matching the optical lengths of the LO and the probe path to eliminate laser phase noise during photodetection [33]. However, this method requires a high-accuracy optical fiber transfer delay measurement and control module, which consequently increases the complexity of the measurement system. Besides, this method is unsuitable for unknown delay situations. In summary, existing MWP-based coherent OVA systems are designed primarily for specific scenarios. In practical application, the requirement of active calibration or elimination of phase noise during measurement cannot be avoided. A universal and flexible measurement method for coherent OVA systems has yet to be developed.

In this article, we introduce a self-calibrated coherent OVA system utilizing MWP technology, which offers superior frequency resolution and sensitivity. The system employs a probe and an LO signal, each characterized as a frequency-swept double-sideband signal at different frequencies. After coherent detection, common-mode laser phase noise within the photocurrent's frequency components is efficiently removed in the digital domain by employing a self-calibration architecture. To avoid aliasing of the double-sideband signal during the extraction of the DUT response, we propose a novel two-step measurement method that accurately obtains the group delay response of the DUT. In comparison to traditional coherent measurement, the self-calibration architecture eliminates extra errors from the external reference and simplifies the system's complexity. Benefiting from the fine frequency sweeping of the MWP techniques, the proposed measurement system can achieve theoretical frequency resolution at the hertz level. The performance is verified by measuring the responses of both a gas cell and an on-chip microring.

II. Principle

The schematic of the coherent OVA system based on MWP is depicted in Fig. 1. The system initiates with an optical carrier signal of frequency ω_o, emitted by a laser. An optical coupler (OC) splits this carrier signal into two

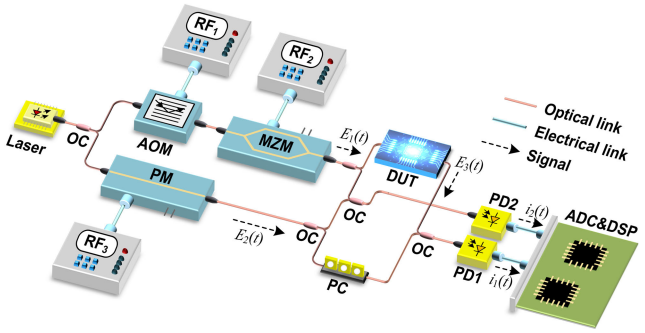

Fig. 1. Configuration of the coherent OVA system based on MWP. OC: optical coupler, AOM: acousto-optic modulator, PM: phase modulator, MZM: Mach–Zehnder modulator, RF: radio frequency, DUT: device under test, PC: polarization controller, PD: photodetector, ADC: analog-to-digital convertor, and DSP: digital signal processor.

distinct branches. In one branch, an acousto-optic modulator (AOM) facilitates the frequency shift of the optical signal ω_{FS}. The signal is then modulated by an ω_1 radio frequency (denoted as RF_2 in Fig. 1) using a Mach–Zehnder modulator (MZM). This modulation process results in the generation of a carrier-suppressed double-sideband (CS-DSB) optical signal.

$$E_1(t) = M_1 \cdot \exp j[(\omega_o + \omega_{\mathrm{FS}})t + \varphi(t)] \cdot 2\cos(\omega_1 t) \tag{1}$$

where M_1 represents the sideband amplitude at the $\pm$1st order in the modulated signal, and $\varphi(t)$ denotes the time-dependent phase variation of the optical carrier resulting from laser phase noise.

In the other branch, the optical signal is modulated by a phase modulator (PM). This modulation can be expressed as follows:

$$E_2(t) = \exp j[\omega_o(t-\tau_0) + \varphi(t-\tau_0)] \cdot \left[jB_1 \exp j(\omega_2(t-\tau_0)) + B_0 - jB_1 \exp j(-\omega_2(t-\tau_0)) \right] \tag{2}$$

where τ_0 is the delay difference between the two branches, B_n represents the amplitude of the sideband at the nth order in the modulated signal, and $\omega_2 < \omega_1 - \omega_{\mathrm{FS}}$ is the frequency of RF_3. The three RF signals are phase-locked to the same reference source.

The system uses the phase-modulated signal as the LO signal, while the CS-DSB signal acts as the probe signal. After the probe signal passes through the DUT, it carries the information of the frequency response, which can be expressed as follows:

$$E_3(t) = \exp j[(\omega_o + \omega_{\mathrm{FS}})(t-\tau_d) + \varphi(t-\tau_d)] \cdot \sum_{n=-1}^{n=1} \frac{1}{2} M_{|n|} H(\omega_o + \omega_{\mathrm{FS}} + n\omega_1) \cdot \exp(jn\omega_1(t-\tau_d)) \tag{3}$$

where $H(\omega)$ is the frequency response of the DUT at the specific frequency of ω, $M_0 = 0$, and τ_d is the delay difference between the link containing the DUT and the link that includes the polarization controller (PC). The probe signal and the LO signal are then detected by the photodetector, denoted PD_1 in Fig. 1. In the article, we exclusively focus on the two

Authorized licensed use limited to: NANJING UNIVERSITY OF AERONAUTICS AND ASTRONAUTICS. Downloaded on August 19,2025 at 09:01:27 UTC from IEEE Xplore. Restrictions apply.

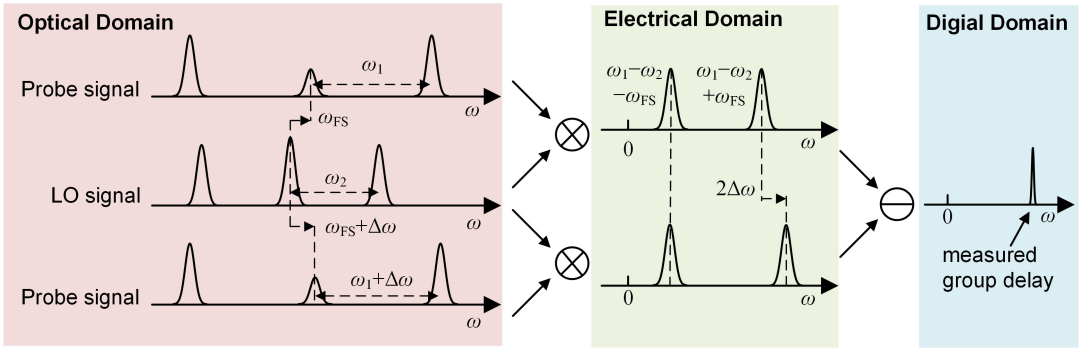

Fig. 2. Optical and electrical signal spectra in the self-calibrated coherent OVA system during the two-step measurement process.

components, $\omega_1-\omega_2+\omega_{\rm FS}$ and $\omega_1-\omega_2-\omega_{\rm FS}$. The photocurrent is as follows:

$$\begin{aligned} i_1(t) &= |E_2(t)+E_3(t)|^2 \\ &= \frac{1}{2}\eta M_1 B_1\{H(\omega_o+\omega_{\rm FS}+\omega_1)\cdot \exp j[(\omega_1+\omega_{\rm FS}-\omega_2)t \\ &\quad -(\omega_1+\omega_{\rm FS}+\omega_o)\tau_d+(\omega_o+\omega_2)\tau_0 \\ &\quad +\varphi(t-\tau_d)-\varphi(t-\tau_0)] \\ &\quad + H^*(\omega_o+\omega_{\rm FS}-\omega_1)\cdot \exp j[(\omega_1-\omega_{\rm FS}-\omega_2)t \\ &\quad -(\omega_1-\omega_{\rm FS}-\omega_o)\tau_d-(\omega_o-\omega_2)\tau_0 \\ &\quad -\varphi(t-\tau_d)+\varphi(t-\tau_0)]\} \end{aligned} \tag{4}$$

where η is the responsivity of the photodetector. Similarly, PD_2 detects the combination of the CS-DSB signal without passing through the DUT. The phase-modulated signal can be described as follows:

$$\begin{aligned} i_2(t) &= |E_1(t)+E_2(t)|^2 \\ &= \frac{1}{2}\eta M_1 B_1\{\exp j[(\omega_1+\omega_{\rm FS}-\omega_2)t \\ &\quad +(\omega_o+\omega_2)\tau_0+\varphi(t)-\varphi(t-\tau_0)] \\ &\quad +\exp j[(\omega_1-\omega_{\rm FS}-\omega_2)t-(\omega_o-\omega_2)\tau_0 \\ &\quad -\varphi(t)+\varphi(t-\tau_0)]\}. \end{aligned} \tag{5}$$

Since two photocurrents have identical frequency components, we can subsequently extract their amplitudes and phase differences using an analog-to-digital converter (ADC) and digital signal processor (DSP):

$$\begin{aligned} \theta(\omega_1+\omega_{\rm FS}-\omega_2) &= \angle H(\omega_o+\omega_{\rm FS}+\omega_1) \\ &\quad -(\omega_1+\omega_{\rm FS}+\omega_o)\tau_d+\varphi(t-\tau_d)-\varphi(t) \end{aligned} \tag{6}$$

$$\begin{aligned} \theta(\omega_1-\omega_{\rm FS}-\omega_2) &= \angle H^*(\omega_o+\omega_{\rm FS}-\omega_1) \\ &\quad -(\omega_1-\omega_{\rm FS}-\omega_o)\tau_d-\varphi(t-\tau_d)+\varphi(t) \end{aligned} \tag{7}$$

$$A(\omega_1+\omega_{\rm FS}-\omega_2) = |H(\omega_o+\omega_{\rm FS}+\omega_1)| \tag{8}$$

$$A(\omega_1-\omega_{\rm FS}-\omega_2) = |H(\omega_o+\omega_{\rm FS}-\omega_1)|. \tag{9}$$

where $\theta(\omega)$ and $A(\omega)$ are the extracted phase and amplitude differences between the two photocurrents at the frequency component ω, while $\angle H(\omega)$ is the phase response of the DUT at the frequency ω. We can obtain the results of the magnitude response measurement using (8) and (9). Nevertheless, the phase responses incorporate several time-varying parameters that influence the measurement. Next, we will present a two-step method for eliminating these error parameters.

For the phase response measurement, it can be seen that (6) and (7) share a common error term: $\varphi(t-\tau_d)-\varphi(t)-(\omega_o+\omega_{\rm FS})\tau_d$, which can be eliminated in the digital domain.

$$\begin{aligned} \Phi_1 &= \theta(\omega_1+\omega_{\rm FS}-\omega_2)+\theta(\omega_1-\omega_{\rm FS}-\omega_2) \\ &= \angle H(\omega_o+\omega_{\rm FS}+\omega_1)+\angle H^*(\omega_o+\omega_{\rm FS}-\omega_1)-2\omega_1\tau_d. \end{aligned} \tag{10}$$

Although the optical carrier phase noise and phase shift are removed, the obtained Φ_1 still contains both the +1st and −1st sidebands and cannot be separated. Here, we employ a two-step measurement process. The modulation frequency of the AOM is changed to $\omega_{\rm FS}+\Delta\omega$, while RF_1 is changed to $\omega_1+\Delta\omega$. Equation (10) can then be rewritten as follows:

$$\begin{aligned} \Phi_2 &= \theta(\omega_1+\omega_{\rm FS}-\omega_2+2\Delta\omega)+\theta(\omega_1-\omega_{\rm FS}-\omega_2) \\ &= \angle H(\omega_o+\omega_{\rm FS}+\omega_1+2\Delta\omega) \\ &\quad +\angle H(\omega_o+\omega_{\rm FS}-\omega_1)-2(\omega_1+\Delta\omega)\tau_d. \end{aligned} \tag{11}$$

The signal spectra during the two-step measurement process are illustrated in Fig. 2. In this figure, the probe signal encompasses the spectra of both $E_1(t)$ and $E_3(t)$, while the LO signal corresponds to the spectrum of $E_2(t)$. Given that the group delay is defined as the derivative of phase with respect to frequency, we can calculate the group delay response using (10) and (11).

$$\begin{aligned} \Phi_2-\Phi_1 &= \theta(\omega_1+\omega_{\rm FS}-\omega_2+2\Delta\omega)-\theta(\omega_1+\omega_{\rm FS}-\omega_2) \\ &= \angle H(\omega_o+\omega_{\rm FS}+\omega_1+2\Delta\omega) \\ &\quad -\angle H(\omega_o+\omega_{\rm FS}+\omega_1)-2\Delta\omega\tau_d \\ &\approx 2\Delta\omega\cdot[GD(\omega_o+\omega_{\rm FS}+\omega_1+\Delta\omega)-\tau_d] \end{aligned} \tag{12}$$

where $GD(\omega)$ is the group delay response of the DUT at the specific frequency of ω. It should be noted that the delay τ_d is a constant, encompassing both the optical fiber pigtail and the transfer delay of the DUT. In numerous instances, the transfer delay is incorporated into the group delay, as it conveys information about the DUT's length. In this article, the fixed delay τ_d is excluded from the results.

III. Experiment and Discussion

In the experiment, we establish the self-calibrated coherent OVA system, as illustrated in Fig. 1. The hardware implementation of this system is shown in Fig. 3. The optical carrier

Authorized licensed use limited to: NANJING UNIVERSITY OF AERONAUTICS AND ASTRONAUTICS. Downloaded on August 19,2025 at 09:01:27 UTC from IEEE Xplore. Restrictions apply.

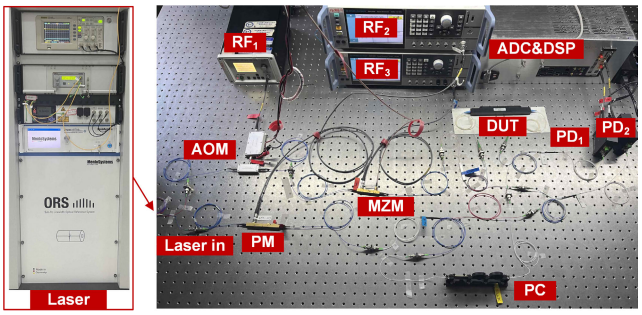

Fig. 3. Hardware system of the self-calibrated coherent OVA.

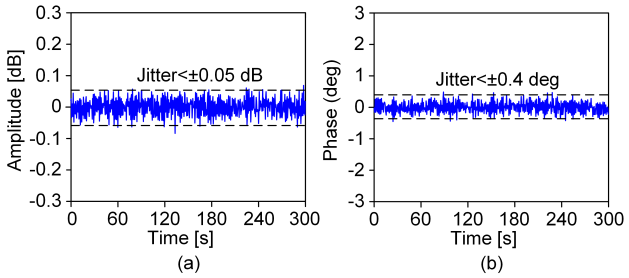

Fig. 4. Stability of the system's (a) amplitude and (b) phase at a 6 GHz frequency point over 300 s with a received optical probe signal power of –50 dBm.

is emitted from an ultrastable laser (Menlo, ORS), which is locked to a high-finesse Fabry–Perot cavity. The carrier is then divided into two branches. For generating the CS-DSB signal, the optical signal is modulated by an 80-MHz AOM (Gooch&Housego Inc.) and a 40-GHz MZM (Eospace, AX-0MVS-40). The modulation is driven by signals from RF1 (Anapico, APSIN26G) and RF2 (R&S, SMA100B), corresponding to each modulator, respectively. The optical signal is modulated by a 40-GHz PM (Eospace, PM-5VEK-40-PFA) to generate the phase-modulated signal. The driving signal for this modulation is provided by RF3 (R&S, SMA100B). In implementing a two-step measurement, the frequencies of RF2 are set separately at 79 and 81 MHz, resulting in a frequency difference of $\Delta\omega = 2$ MHz. Similarly, the frequency differences between RF2 and RF3 are adjusted to 97 and 99 MHz. Two 1.6-GHz photodetectors (Thorlabs, PDB480C) are employed to detect the combination of these modulated optical signals. An ADC card (Teledyne, SPD ADQ14) with a 14-bit resolution and a sampling rate of 1 GSa/s is utilized for data acquisition.

In the first measurement, the objective is to extract the amplitude and phase of photocurrent frequencies at 18 and 176 MHz. The photocurrent with 18- and 180-MHz frequencies is analyzed for the second measurement. According to the principle, we can achieve a frequency aperture of 4 MHz for the group delay response measurement. The extraction of the signal's amplitude and phase extraction is achieved within the digital domain by employing the fast Fourier transform (FFT).

A. Analysis of Error and Enhancement of Sensitivity

Generally, the measurement error can be evaluated using the mean squared error (mse). For the parameter T to be estimated, the mse is given by $\text{mse}(T) = \text{var}(T) + (\text{bias}(T))^2$, where $\text{var}(T)$ represents the variance of the measurement, and $\text{bias}(T)$ denotes the fixed bias of the measurement.

From the perspective of measurement bias, if only white noise is considered in the system, the proposed method based on the reception of the intermediate frequency (IF) signal in the digital domain is an unbiased estimator [43]. Before measurement, the system is fully calibrated to eliminate systematic bias [44]. In practical measurements, external factors such as environmental temperature fluctuations, platform vibrations, and laser frequency drift may introduce additional errors [45]. Therefore, the measurement system is temperature-controlled and installed on a vibration isolation platform, effectively eliminating external environmental disturbances. Additionally, the laser used in our system is strictly frequency-locked to a vacuum chamber, with a long-term frequency drift of less than 1 Hz, making the resulting measurement error negligible. To further illustrate the stability of our system, the stability of the system at a 6-GHz frequency point with a received optical probe signal power of -50 dBm is measured over 300 s. As illustrated in Fig. 4, the measured amplitude and phase exhibited stability within ± 0.05 dB and $\pm 0.4°$, indicating that no additional bias was introduced during the measurement process. Further comparison of the accuracy between our measured results and other methods will be given in the following subsection.

With respect to variance, it is mainly determined by the signal-to-noise ratio (SNR) of the received signal and the duration of sampling [46]. The photocurrent signal can generally be represented as $s(t) = b_0 \cos(\omega_0 t + \theta_0)$, where b_0 and θ_0 are the parameters that we aim to extract in the OVA system. The accuracy of these estimations is fundamentally limited by the Cramer–Rao lower bound (CRLB), which can be expressed as follows:

$$\text{var}(\hat{b}) \geq \frac{\sigma^2}{N} = b_0^2 \cdot \frac{1}{\text{SNR} \cdot N} \tag{13}$$

$$\text{var}(\hat{\theta}) \geq \frac{\sigma^2}{b_0^2 \cdot N} = \frac{1}{\text{SNR} \cdot N} \tag{14}$$

where N is the sampling number, σ^2 is the variance of received white noise, and SNR is defined as σ^2/b_0^2. The noise in the system [47] consists mainly of relative intensity noise, shot noise, thermal noise, and quantization noise. When it comes to a coherent system, the laser phase noise should also be considered. All of these noises can be seen as independent variables. The sum of these variances contributes to the total variance σ^2.

The photodetectors operate based on square-law detection, resulting in a quadratic decrease in the SNR of the incoherent OVA system as the optical power decreases linearly. However, in the coherent OVA system, the sensitivity of the receiver can be improved via power compensation from the LO signal. Consequently, the SNR of the measurement signal is directly proportional to the power of the probe signal. This distinctive feature provides enhanced sensitivity with the OVA system.

To validate sensitivity enhancement, we establish a typical incoherent OVA system based on MWP technology,

Authorized licensed use limited to: NANJING UNIVERSITY OF AERONAUTICS AND ASTRONAUTICS. Downloaded on August 19,2025 at 09:01:27 UTC from IEEE Xplore. Restrictions apply.

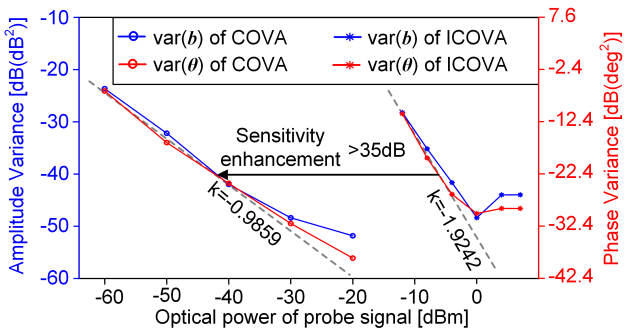

Fig. 5. Comparison of the sensitivity between the coherent and incoherent OVA. COVA: proposed coherent OVA, ICOVA: incoherent OVA, and k is the slope of the fitted line.

as described in [23], for comparison. In the incoherent system, all devices are identical to those in the coherent system, except for two key differences: the use of two 40-GHz photodetectors (Finisar, XPDV2120R) and a different receiver (R&S, ZVA67). Both the frequency resolution and aperture settings in the incoherent system match those of the coherent OVA system. The DUT comprises a variable optical attenuator (EXFO, FVA-600) and a 1-m optical fiber. The optical attenuator allows for precise control over the power of the probe signal with a resolution of 0.01 dB. The two OVA systems measure the frequency response covering 6–6.5 GHz. As indicated in Fig. 5, the variances obtained by the two OVA systems are compared. In logarithmic coordinates, the variance is shown to be proportional to the power of the probe signal, provided the receiver is operating within its linear region. The slopes of the fitted lines are −0.9859 and −1.9242, respectively, indicating a twofold relationship. This outcome is consistent with the square-law detection principle of the photodetector. Using a 0.01-dB fluctuation as a criterion in Fig. 5, the proposed coherent OVA system exhibits a sensitivity improvement of at least 35 dB over the incoherent system.

Furthermore, a hydrogen cyanide ($H^{13}C^{14}N$) gas cell (Wavelength References, HCN-13-H(16.5)-25-FCAPC) is used as the DUT to compare the measurement results between the two MWP-based OVA. The center frequency of the optical carrier is set to measure the P11 line of the $2v_3$ rotational–vibrational combination band. The probe signal is maintained at a power level of −50 dBm in the coherent OVA system. For comparison, the incoherent OVA system measures the gas cell with the probe signal at −8 dBm. The responses measured in the range of 6–30 GHz, with a frequency resolution of 10 MHz, are illustrated in Fig. 6. The absorption peak, namely the P11 line, is identified at approximately 1550.515 nm. Both methods displayed similar response fluctuations near 6 GHz, with a magnitude of approximately ±0.05 dB and a group delay of ±6 ps. However, as the RF extends beyond 25 GHz, the incoherent OVA system exhibits a rapid increase in fluctuation, reaching ±0.3 dB in magnitude and ±40 ps in group delay. The error increase is attributed to the traditional receiver's diminished performance at higher frequencies. In contrast, system performance remains consistent across the entire frequency range; thanks to our method's fixed IF reception. In addition, the probe signal power in our method registers

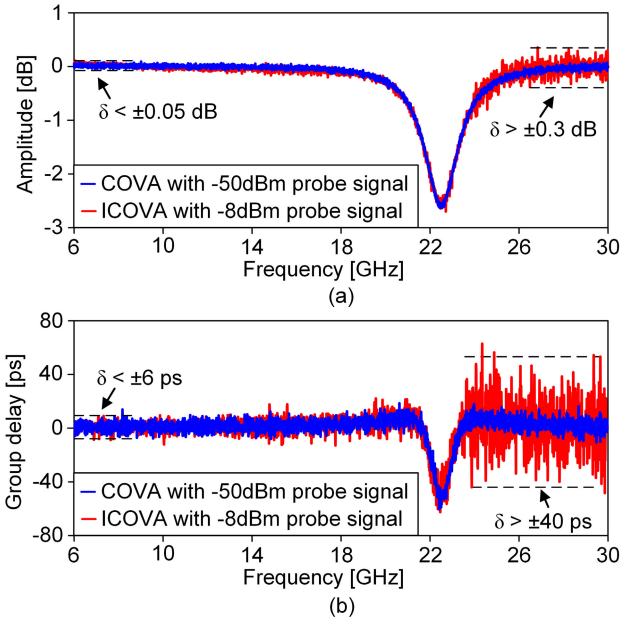

Fig. 6. Measured (a) magnitude response and (b) group delay response of the $H^{13}C^{14}N$ gas cell around 1550.5 nm. δ is the measurement fluctuation.

a decrease of more than 42 dB compared to the conventional OVA system, showing a significant improvement in sensitivity.

B. Frequency Resolution

To demonstrate frequency resolution and measurement accuracy, we compare the proposed OVA system with a commercial coherent OVA product (LUNA, OVA5000), as referenced in [42]. Traditional commercial coherent OVA products typically utilize an interferometry approach with a relatively low-frequency resolution (approximately 150 MHz at 1550 nm). The laser is locked to a stable cavity in our proposed coherent OVA system. This design facilitates the use of fine microwave sweeping techniques, enabling our system to achieve a significantly higher frequency resolution.

Fig. 7 presents the measured magnitude and group delay response of the $H^{13}C^{14}N$ gas cell at varying power levels of the probe signal. The inner box of the figure provides detailed results of the absorption peak measurement. The absorption peak measured by OVA5000 only contains several frequency points. Although higher frequency resolution can be achieved through response curve fitting, it is important to note that low power levels of the probe signal significantly influence the fitting process. Our proposed coherent OVA demonstrates outstanding consistency in magnitude response measurements, with peak deviations below 0.007 dB. In contrast, the OVA5000 shows peak deviations that exceed 0.03 dB. In group delay measurement, the OVA5000 has difficulty accurately characterizing the absorption peak when the optical power level drops below −40 dBm. This limitation is not only due to the system's low-frequency resolution but also a consequence of the broadband receiver used in its swept-frequency method. In particular, even with results averaged more than 50 times, the SNR of the OVA5000 does not effectively enhance when the probe signal has a relatively low

Authorized licensed use limited to: NANJING UNIVERSITY OF AERONAUTICS AND ASTRONAUTICS. Downloaded on August 19,2025 at 09:01:27 UTC from IEEE Xplore. Restrictions apply.

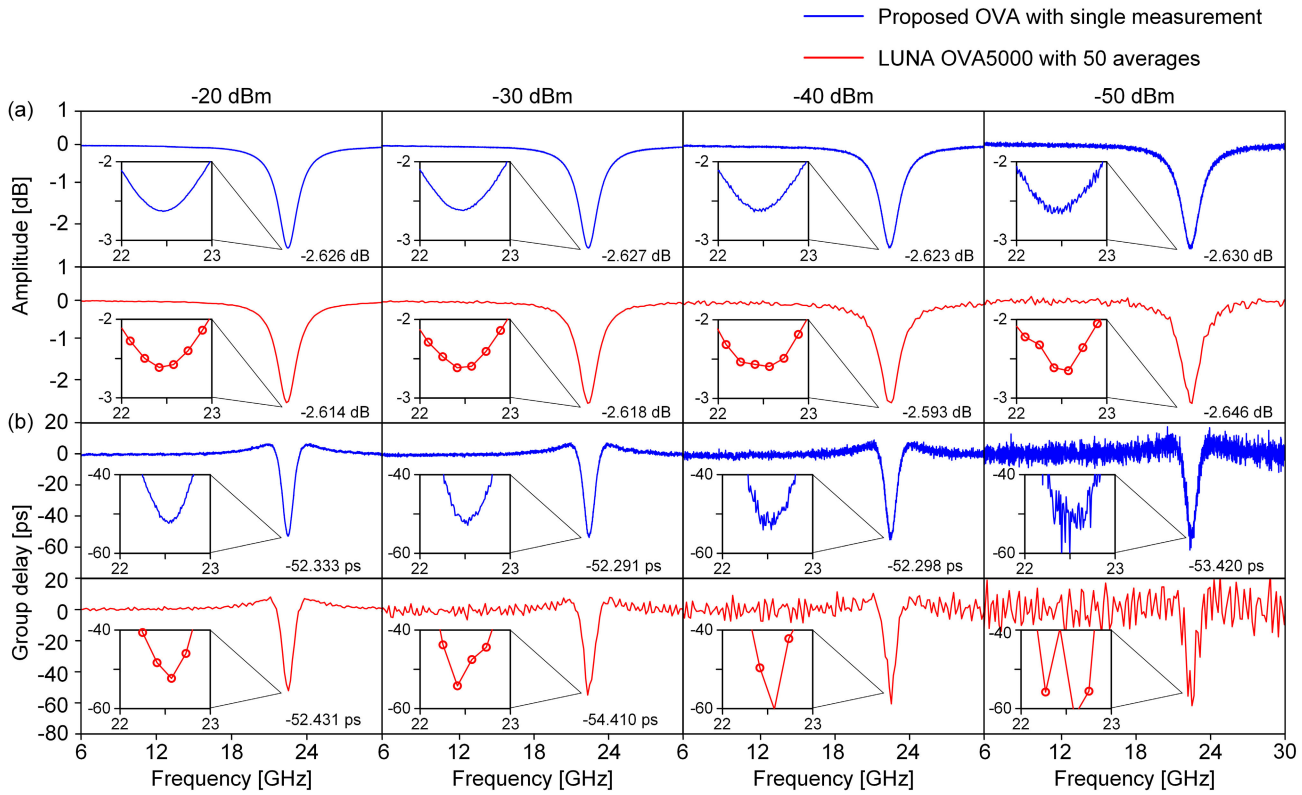

Fig. 7. Measured (a) magnitude response and (b) group delay response of the $H^{13}C^{14}N$ gas cell under different power of probe signal.

power level. Above all, our proposed method offers higher frequency resolution and better accuracy than the commercial coherent OVA product. The limit of frequency resolution in our system is fundamentally determined by the linewidth, which in theory can reach down to the hertz level.

To show the ability of high-frequency resolution, we also measure an on-chip Si_3N_4 microring resonator using the proposed OVA method and incoherent OVA methods [23]. The resonator used in this experiment has a quality factor of approximately 2×10^6, corresponding to a 3-dB bandwidth of 100 MHz. The LUNA5000, with its limited frequency resolution of 150 MHz, cannot measure the response of the resonant peak in this case. Additionally, the total insertion loss of the resonator is over 10 dB. The frequency resolution and the frequency aperture in this experiment are set at 1 MHz. Fig. 8 shows the measured resonance peak responses of the Si_3N_4 microring resonator, with part (a) encompassing a frequency range of 1 GHz and part (b) focusing on a narrower range of 100 MHz. Fig. 8(b) offers an enlarged view of the area highlighted by the green box in Fig. 8(a). The results of the proposed coherent OVA system demonstrate a performance enhancement in magnitude fluctuation. However, it should be noted that the fluctuation in the measured group delay near the resonant peak exceeds 10 ns. This is because the loss reaches its maximum at the resonant peak and the SNR is at its minimum.

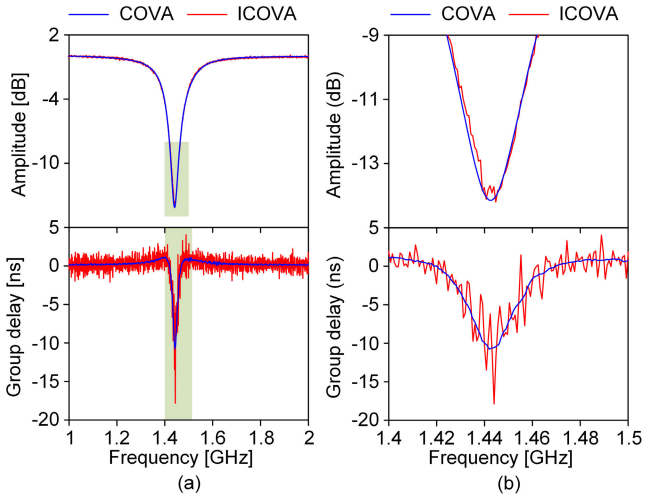

Fig. 8. Measured resonate peak responses of a Si_3N_4 microring resonator covering (a) 1 GHz and (b) 100 MHz. The blue line indicates the results measured by coherent OVA. The red line indicates the results measured by incoherent OVA.

C. Influence of the Coherence

The coherence between the LO signal and the probe signal, determined by the laser linewidth Δf and relative delay τ_d, plays a pivotal role in the performance of the coherent OVA system. Given that laser phase noise is a stochastic variable, we conducted two simulations to assess its influence on system performance. These simulations are performed using the OptiSystem platform, with relative parameters provided in Table I. The frequencies of the photocurrent were consistent with those used in our experiments. Fig. 9(a) illustrates the relationship between photocurrent phase fluctuation and laser coherence, where the relative delay is fixed at 1 μs while the

Authorized licensed use limited to: NANJING UNIVERSITY OF AERONAUTICS AND ASTRONAUTICS. Downloaded on August 19,2025 at 09:01:27 UTC from IEEE Xplore. Restrictions apply.

TABLE I
SIMULATION PARAMETERS FOR COHERENT OVA

Parameter	Value
Laser output power	0 dBm
Modulator extinction ratio	30 dB
PD responsivity	1 A/W
PD dark current	10 nA
PD 3 dB bandwidth	2 GHz
PD thermal power density	10^{22} W/Hz
ADC dynamic range	100 dB
Sampling rate	10 GSa/s
Sampling time width	0.5 ms

laser linewidth is varied from 10 Hz to 10 MHz. It is observed that the traditional coherent OVA systems exhibit improved phase stability when employing ultranarrow linewidth laser. This enhancement is attributed to our method, which employs a differential process to mitigate laser phase noise. Consequently, the phase fluctuation induced by receiver noise in our system is twice that of traditional OVA systems. With poorer laser coherence, the phase fluctuation in traditional coherent OVA systems becomes proportional to the laser coherence. In contrast, our method maintains stable phase detection accuracy across a broad range of laser linewidths. When laser coherence is significantly reduced, the coherent gain provided by the LO signal diminishes, leading to a deterioration in the SNR. Under these conditions, the additional phase fluctuation arises from receiver noise. Fig. 9(b) demonstrates a similar phenomenon when the laser linewidth Δf is fixed at 10 kHz, while the relative delay τ_d is varied from 0.1 ns to 0.1 ms. The results of both simulations substantiate the superior stability of our method in measuring group delay responses compared to traditional coherent OVA systems. Furthermore, we can categorize these results into three regions based on laser coherence. As long as the coherent gain has not significantly decreased, which occurs when the product of the relative delay and laser linewidth is less than 10^{-1}, our proposed method does not experience any loss in phase detection accuracy due to laser phase noise.

Next, we explore the relationship between coherent gain loss and coherence. A mathematical model constructed based on a stochastic process elucidates this relationship. The probability distribution of the laser phase noise, $\varphi(t)$, is modeled as a normal distribution. For analysis, we consider the time average to represent the stochastic process. Only one frequency component to be extracted is considered. According to (4), the power spectrum density (PSD) of the photocurrent frequency component can be derived using the Wiener–Khintchine theorem, which relates the PSD to the autocorrelation function of the photocurrent as follows:

$$S(\delta\omega) = \frac{1}{2}P_0 P\pi \exp\left(-\frac{\tau_d}{\tau_c}\right)\delta(\delta\omega) + \frac{P_0 P\tau_c}{1+(\delta\omega)^2\tau_c^2} \times \left\{1-\exp\left(-\frac{\tau_d}{\tau_c}\right)\left[\cos(\delta\omega)\tau_d + \frac{\tau_d}{\tau_c}\mathrm{sinc}(\delta\omega)\tau_d\right]\right\} \quad (15)$$

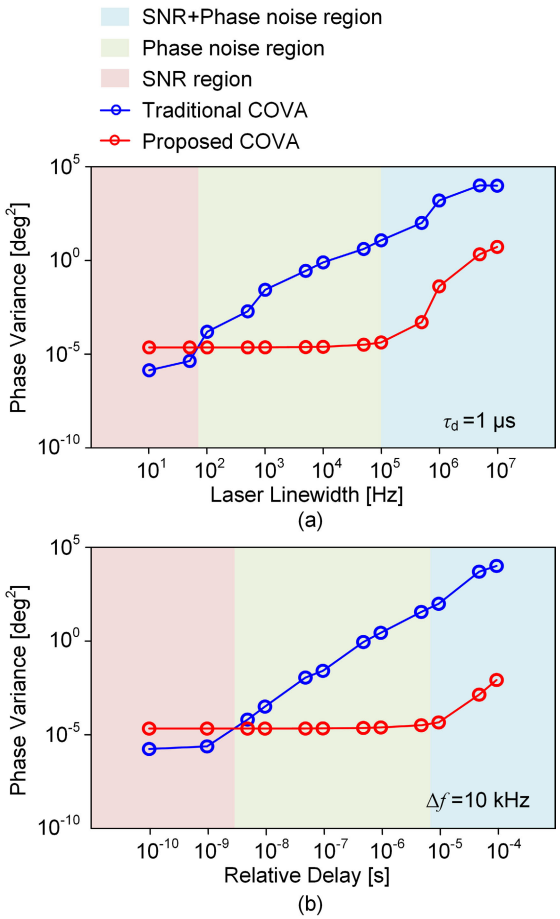

Fig. 9. Simulation results of the phase variance concerning coherence. (a) Relative delay is fixed at 1 μs while the laser linewidth is swept from 10 Hz to 10 MHz. (b) Laser linewidth is fixed at 10 kHz while the relative delay is swept from 0.1 ns to 0.1 ms. The phase detection accuracy in three regions depends on its dominating factors.

where P_0 and P are the power of the LO signal and the probe signal, respectively, $\tau_c = 1/\Delta f$ is the coherence time of the laser, $\delta\omega = \omega - \Omega$ is the frequency component to be extracted, $\delta(\cdot)$ and $\mathrm{sinc}(\cdot)$ are the Dirac delta function and the sine cardinal function, respectively. Equation (15) shows that the PSD includes terms that involve the Dirac delta, Lorentzian, and trigonometric functions. Fig. 10(a) is a schematic demonstrating the coherent gain loss induced by the different coherence. When $\tau_d \ll \tau_c$, the power is predominantly concentrated around the Dirac delta function, indicating high coherence between the LO and probe signals. As τ_d increases, the value of the Dirac delta function decreases while that of the Lorentzian function increases. When $\tau_d \gg \tau_c$, the coherence between the LO signal and the probe signals is completely degraded, resulting in the photocurrent spectrum resembling a Lorentz curve with a linewidth of $2\Delta f$, because $\exp(-\tau_d/\tau_c) \to 0$. Fig. 10(b) illustrates the coherent gain loss induced by the laser linewidth and relative delay. We introduce a parameter $C(-G)$ to quantify the gain loss under varying coherence conditions, where G represents the coherent gain loss, and C denotes the relative delay and the laser linewidth product. It is evident that to maintain an amplitude loss of

Authorized licensed use limited to: NANJING UNIVERSITY OF AERONAUTICS AND ASTRONAUTICS. Downloaded on August 19,2025 at 09:01:27 UTC from IEEE Xplore. Restrictions apply.

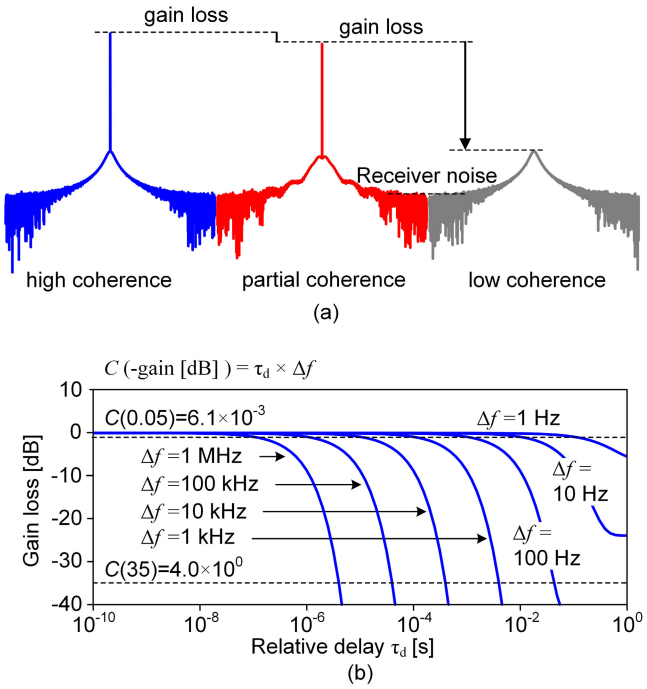

Fig. 10. (a) Photocurrent spectrums in coherent detection under different coherence conditions. (b) Coherent gain loss due to phase noise, plotted versus relative delay τ_d, where τ_d is the delay between the LO link and probe link.

less than 0.05 dB, the product of the relative delay and laser linewidth should be less than 6.1×10^{-3}. This indicates that, using the same receiver to measure a low-loss DUT, the proposed method may yield inferior measurement results compared to the incoherent OVA method if the relative delay exceeds $6.1 \times 10^{-3}/\Delta f$. In our experiments, we validate that when measuring a DUT with significant insertion loss, our method achieves a sensitivity enhancement of at least 35 dB when measuring a DUT with significant insertion loss. Under these circumstances, the constraint on the relative delay can be relaxed to $4.0/\Delta f$.

IV. Conclusion

This article presents a novel self-calibrated MWP-based coherent OVA system, incorporating a two-step measurement methodology to effectively eliminate laser phase noise in coherent detection. The system is specifically designed to characterize optical devices that comply with stringent requirements concerning high sensitivity and narrow bandwidth. This proposed system exhibits considerable performance advantages compared to conventional methodologies. The experimental results are compared with both state-of-the-art traditional OVA systems and commercial coherent OVA products; our system demonstrates three significant performance advantages.

1) An exceptional enhancement in sensitivity surpassing 35 dB when compared to traditional incoherent OVA methods.
2) An improvement in frequency resolution by several orders of magnitude relative to conventional coherent OVA techniques.
3) High-accuracy enabled by a superior SNR achieved via MWP-enabled electrical domain narrow-band IF reception.

These advancements establish the proposed OVA system as a promising solution for two critical applications: integrated optical circuit characterization and high-accuracy spectroscopy. This progress may facilitate new possibilities in the analysis and measurement of photonic devices.

References

[1] S. Kawanishi, A. Takada, and M. Saruwatari, "Wideband frequency-response measurement of optical receivers using optical heterodyne detection," *J. Lightw. Technol.*, vol. 7, no. 1, pp. 92–98, Jan. 1989.
[2] M. Shirazi, R. Zane, and D. Maksimovic, "An autotuning digital controller for DC–DC power converters based on online frequency-response measurement," *IEEE Trans. Power Electron.*, vol. 24, no. 11, pp. 2578–2588, Nov. 2009.
[3] P. D. Hale and D. F. Williams, "Calibrated measurement of optoelectronic frequency response," *IEEE Trans. Microw. Theory Techn.*, vol. 51, no. 4, pp. 1422–1429, Apr. 2003.
[4] M. Xue, M. Lv, Q. Wang, B. Zhu, C. Yu, and S. Pan, "Broadband optoelectronic frequency response measurement utilizing frequency conversion," *IEEE Trans. Instrum. Meas.*, vol. 70, pp. 1–5, 2021.
[5] R. Richards-Kortum and E. Sevick-Muraca, "Quantitative optical spectroscopy for tissue diagnosis," *Annu. Rev. Phys. Chem.*, vol. 47, no. 1, pp. 555–606, Oct. 1996.
[6] J. N. Fernandes et al., "Rapid, noninvasive detection of Zika virus in aedes aegypti mosquitoes by near-infrared spectroscopy," *Sci. Adv.*, vol. 4, no. 5, p. 496, May 2018.
[7] S. Veerasingam et al., "Contributions of Fourier transform infrared spectroscopy in microplastic pollution research: A review," *Crit. Rev. Environ. Sci. Technol.*, vol. 51, no. 22, pp. 2681–2743, Nov. 2021.
[8] D. Yu et al., "Simultaneous CH_4/CO measurement at atmospheric pressure using a single 2.3 μm laser and a dual-gas cross-interference cancellation algorithm," *IEEE Trans. Instrum. Meas.*, vol. 71, pp. 1–9, 2022.
[9] C. Xiang, W. Jin, and J. E. Bowers, "Silicon nitride passive and active photonic integrated circuits: Trends and prospects," *Photon. Res.*, vol. 10, no. 6, pp. A82–A96, 2022.
[10] K. Luke, P. Kharel, C. Reimer, L. He, M. Loncar, and M. Zhang, "Wafer-scale low-loss lithium niobate photonic integrated circuits," *Opt. Exp.*, vol. 28, no. 17, pp. 24452–24458, 2020.
[11] C. Huang et al., "Demonstration of scalable microring weight bank control for large-scale photonic integrated circuits," *APL Photon.*, vol. 5, no. 4, Apr. 2020, Art. no. 040803.
[12] S. Zhang et al., "Nonvolatile reconfigurable terahertz wave modulator," *PhotoniX*, vol. 3, no. 1, p. 7, Mar. 2022.
[13] C. Sun et al., "Tunable narrow-band single-channel add-drop integrated optical filter with ultrawide FSR," *PhotoniX*, vol. 3, no. 1, p. 12, Dec. 2022.
[14] X. Zou et al., "A multifunctional photonic integrated circuit for diverse microwave signal generation, transmission, and processing," *Laser Photon. Rev.*, vol. 13, no. 6, Jun. 2019, Art. no. 1800240.
[15] J. Liu et al., "Photonic microwave generation in the X-and K-band using integrated soliton microcombs," *Nature Photon.*, vol. 14, no. 8, pp. 486–491, 2020.
[16] S. Xu et al., "Optical beamforming system based on polarization manipulation with amplitude–phase coupling suppression," *IEEE Trans. Microw. Theory Techn.*, vol. 71, no. 5, pp. 2215–2221, May 2023.
[17] M. Xue, S. Liu, Q. Ling, Y. Heng, J. Fu, and S. Pan, "Ultrahigh-resolution optoelectronic vector analysis for characterization of high-speed integrated coherent receivers," *IEEE Trans. Instrum. Meas.*, vol. 69, no. 6, pp. 3812–3817, Jun. 2020.
[18] S. AbdElazem and W. Al-Basheer, "Measuring the acceleration due to gravity using an IR transceiver," *Eur. J. Phys.*, vol. 36, no. 4, Jul. 2015, Art. no. 045017.
[19] W. Al-Basheer, T. O. Adigun, A. Aljalal, and K. Gasmi, "Spectral and spatial dynamics of a multimode GaN-based blue laser diode," *J. Mod. Opt.*, vol. 67, no. 4, pp. 355–360, Feb. 2020.
[20] T. Dennis and P. A. Williams, "Achieving high absolute accuracy for group-delay measurements using the modulation phase-shift technique," *J. Lightw. Technol.*, vol. 23, no. 11, pp. 3748–3754, Nov. 2005.

Authorized licensed use limited to: NANJING UNIVERSITY OF AERONAUTICS AND ASTRONAUTICS. Downloaded on August 19,2025 at 09:01:27 UTC from IEEE Xplore. Restrictions apply.

[21] S. Liu, M. Xue, J. Fu, L. Wu, and S. Pan, "Ultrahigh-resolution and wideband optical vector analysis for arbitrary responses," *Opt. Lett.*, vol. 43, no. 4, p. 727, 2018.
[22] S. Pan and M. Xue, "Ultrahigh-resolution optical vector analysis based on optical single-sideband modulation," *J. Lightw. Technol.*, vol. 35, no. 4, pp. 836–845, Feb. 15, 2017.
[23] T. Qing, S. Li, Z. Tang, B. Gao, and S. Pan, "Optical vector analysis with attometer resolution, 90-dB dynamic range and THz bandwidth," *Nature Commun.*, vol. 10, no. 1, p. 5135, Nov. 2019.
[24] D. K. Gifford, B. J. Soller, M. S. Wolfe, and M. E. Froggatt, "Optical vector network analyzer for single-scan measurements of loss, group delay, and polarization mode dispersion," *Appl. Opt.*, vol. 44, no. 34, pp. 7282–7286, 2005.
[25] B. Wang, W. Zhang, and X. Fan, "Self-calibrated optical vector analyzer with a largely extended measurement range based on linearly frequency-modulated waveform and recirculating frequency shifter," *Opt. Exp.*, vol. 28, no. 19, pp. 28536–28547, 2020.
[26] W. Zhang, B. Wang, X. Fan, and S. Zhao, "Ultrahigh-resolution optical vector analyzer for multiple parallel measurements," *Opt. Exp.*, vol. 28, no. 19, pp. 28536–28547, 2020.
[27] B. Wang, X. Fan, S. Zhao, and W. Zhang, "Ultrahigh-resolution optical vector analyzer for multiple parallel measurements based on frequency-domain analysis," *Opt. Lett.*, vol. 47, no. 9, p. 2318, 2022.
[28] Y. Zhang et al., "Ultrafast and wideband optical vector analyzer based on optical dual linear-frequency modulation," *IEEE Photon. Technol. Lett.*, vol. 35, no. 19, pp. 1055–1058, Jul. 26, 2023.
[29] X. Zou et al., "Hyperfine intrinsic magnitude and phase response measurement of optical filters based on electro-optical harmonics heterodyne and Wiener–Lee transformation," *J. Lightw. Technol.*, vol. 37, no. 11, pp. 2654–2660, Jun. 1, 2019.
[30] M. Xue, W. Chen, B. Zhu, and S. Pan, "Ultrahigh-resolution optical vector analysis for arbitrary responses using low-frequency detection," *IEEE Photon. Technol. Lett.*, vol. 30, no. 17, pp. 1523–1526, Sep. 1, 2018.
[31] M. Xue, W. Chen, Y. Heng, T. Qing, and S. Pan, "Ultrahigh-resolution optical vector analysis using fixed low-frequency electrical phase-magnitude detection," *Opt. Lett.*, vol. 43, no. 13, pp. 3041–3044, 2018.
[32] D. Feng, Y. Gao, X. Zhang, T. Zhu, and R. Cao, "Ultra wideband measurement for arbitrary spectral response using double sideband modulation and low-frequency detection," *Opt. Commun.*, vol. 460, Apr. 2020, Art. no. 125198.
[33] T. Qing et al., "High-resolution optical vector analysis with enhanced sensitivity," *IEEE Photon. Technol. Lett.*, vol. 33, no. 11, pp. 581–584, Jun. 1, 2021.
[34] L. He et al., "A high-efficiency nonuniform grating coupler realized with 248-nm optical lithography," *IEEE Photon. Technol. Lett.*, vol. 25, no. 14, pp. 1358–1361, Jul. 15, 2013.
[35] C. Zhu et al., "Silicon integrated microwave photonic beamformer," *Optica*, vol. 7, no. 9, pp. 1162–1170, 2020.
[36] S. Hong, L. Zhang, Y. Wang, M. Zhang, Y. Xie, and D. Dai, "Ultralow-loss compact silicon photonic waveguide spirals and delay lines," *Photon. Res.*, vol. 10, no. 1, pp. 1–7, Jan. 2022.
[37] Q. Zhang et al., "Two-dimensional phased-array receiver based on integrated silicon true time delay lines," *IEEE Trans. Microw. Theory Techn.*, vol. 71, no. 3, pp. 1251–1261, Mar. 2023.
[38] A. Al-Saudi, A. Aljalal, W. Al-Basheer, K. Gasmi, and S. Qari, "Investigation of O_2 line broadening in nanoporous alumina using gas in scattering media absorption spectroscopy," *Appl. Phys. B, Lasers Opt.*, vol. 126, no. 4, pp. 1–7, Apr. 2020.
[39] J. Hodgkinson and R. P. Tatam, "Optical gas sensing: A review," *Meas. Sci. Technol.*, vol. 24, no. 1, Jan. 2013, Art. no. 012004.
[40] B. Wang and J. Mu, "High-speed Si-Ge avalanche photodiodes," *PhotoniX*, vol. 3, no. 1, p. 8, Mar. 2022.
[41] S. Yokoyama, A. Okamoto, T. Araki, and N. Suzuki, "Examination to eliminate undesirable phase delay of an avalanche photodiode (APD) for intensity-modulated light," *Rev. Sci. Instrum.*, vol. 66, no. 11, pp. 5331–5336, Nov. 1995.
[42] (Feb. 15, 2019). *Data-Sheet OVA-5000 V2.1*. [Online]. Available: https://lunainc.com/sites/default/files/assets/files/resource-library/LUNA-Data-Sheet-OVA-5000-V2-1.pdf
[43] R. McDonough, *Detection of Signals in Noise*. New York, NY, USA: Academic, 1995.
[44] T. Qing et al., "Comprehensive vector analysis for electro-optical, opto-electronic, and optical devices," *Opt. Lett.*, vol. 46, no. 8, pp. 1856–1859, 2021.
[45] A. Alenaizan, W. Al-Basheer, and M. M. Musa, "Solvent, temperature and concentration effects on the optical rotatory dispersion of (R)-3-methylcyclohexanone," *J. Mol. Struct.*, vol. 1130, pp. 19–25, Feb. 2017.
[46] D. Rife and R. Boorstyn, "Single tone parameter estimation from discrete-time observations," *IEEE Trans. Inf. Theory*, vol. IT-20, no. 5, pp. 591–598, Sep. 1974.
[47] W. S. Chang, *RF Photonic Technology in Optical Fiber Links*. Cambridge, U.K.: Cambridge Univ. Press, 2002.

Lihan Wang received the B.S. degree from Nanjing University of Aeronautics and Astronautics, Nanjing, China, in 2020, where he is currently pursuing the Ph.D. degree with the National Key Laboratory of Microwave Photonics.

His research interests include microwave photonic measurement and photonic-assisted integrated communication and sensing.

Huashan Yang received the B.S. and M.S. degrees in material physics from Nanjing University, Nanjing, China, in 2015 and 2018, respectively. He is currently pursuing the Ph.D. degree with the National Key Laboratory of Microwave Photonics, Nanjing University of Aeronautics and Astronautics, Nanjing.

His current research interests include dissipative Kerr soliton and microresonator.

Xiangchuan Wang received the B.Eng. degree in automation and the Ph.D. degree in microelectronics and solid-state electronics from Nanjing University, Nanjing, China, in 2009 and 2015, respectively.

He is currently a Professor with the National Key Laboratory of Microwave Photonics, Nanjing University of Aeronautics and Astronautics, Nanjing. He has authored or co-authored more than 80 research papers. His current research interests include microwave photonic measurement and optical fiber sensing technologies.

Xiaohu Tang received the B.S. degree from Nanjing University of Aeronautics and Astronautics, Nanjing, China, in 2020, where he is currently pursuing the Ph.D. degree with the National Key Laboratory of Microwave Photonics.

His current research interests include microwave photonic measurement and photonic sampling.

Authorized licensed use limited to: NANJING UNIVERSITY OF AERONAUTICS AND ASTRONAUTICS. Downloaded on August 19,2025 at 09:01:27 UTC from IEEE Xplore. Restrictions apply.

Jingxian Wang received the B.S. degree from Nanchang Hangkong University, Nanchang, China, in 2022. She is currently pursuing the M.Eng. degree with the National Key Laboratory of Microwave Photonics, Nanjing University of Aeronautics and Astronautics, Nanjing, China.

Her research interest includes microwave photonics measurement.

Qianwen Sang received the B.S. degree from China University of Mining and Technology, Xuzhou, China, in 2023. She is currently pursuing the M.Eng. degree with the National Key Laboratory of Microwave Photonics, Nanjing University of Aeronautics and Astronautics, Nanjing, China.

Her research interests include microwave photonic LiDAR.

Min Xue received the B.S. and Ph.D. degrees in electronics engineering from Nanjing University of Aeronautics and Astronautics, Nanjing, China, in 2011 and 2016, respectively.

He joined the College of Electronic and Information Engineering, Nanjing University of Aeronautics and Astronautics, in 2016, where he is currently a member of the National Key Laboratory of Microwave Photonics. His research interests include photonic microwave measurement and metrology, optical fiber sensors, and integrated microwave photonics.

Dr. Xue was awarded with "Hong Kong Scholars" in 2018 and the Gold Medal with the congratulations of the jury in the 45th International Exhibition of Inventions of Geneva in 2017.

Shilong Pan (Fellow, IEEE) received the B.S. and Ph.D. degrees in electronics engineering from Tsinghua University, Beijing, China, in 2004 and 2008, respectively.

From 2008 to 2010, he was a "Vision 2010" Post-Doctoral Research Fellow with the Microwave Photonics Research Laboratory, University of Ottawa, Ottawa, ON, Canada. He joined the College of Electronic and Information Engineering, Nanjing University of Aeronautics and Astronautics, Nanjing, China, in 2010, where he is currently a Full Professor and the Executive Director of the National Key Laboratory of Microwave Photonics. He has authored or co-authored over 380 research papers, including more than 200 papers in peer-reviewed journals and 180 papers in conference proceedings. His research has focused on microwave photonics, which includes optical generation and processing of microwave signals, analog photonic links, photonic microwave measurement, and integrated microwave photonics.

Dr. Pan is a fellow of IET, OSA, and SPIE. He was a recipient of the OSA Outstanding Reviewer Award in 2015 and a Top Reviewer of IEEE/OSA JOURNAL OF LIGHTWAVE TECHNOLOGY in 2016. He was also a recipient of the Excellent Young Scholars Award of the National Natural Science Foundation of China in 2014 and the Scientific and Technological Innovation Leading Talents Award of the National Ten Thousand Plan in 2018.

Authorized licensed use limited to: NANJING UNIVERSITY OF AERONAUTICS AND ASTRONAUTICS. Downloaded on August 19,2025 at 09:01:27 UTC from IEEE Xplore. Restrictions apply.